

MLLM-based Discovery of Intrinsic Coordinates and Governing Equations from High-Dimensional Data

Ruikun Li, Yan Lu*, Shixiang Tang, Biqing Qi, Wanli Ouyang

¹ Shanghai Artificial Intelligence Laboratory

Abstract

Discovering governing equations from scientific data is crucial for understanding the evolution of systems, and is typically framed as a search problem within a candidate equation space. However, the high-dimensional nature of dynamical systems leads to an exponentially expanding equation space, making the search process extremely challenging. The visual perception and pre-trained scientific knowledge of multimodal large language models (MLLM) hold promise for providing effective navigation in high-dimensional equation spaces. In this paper, we propose a zero-shot method based on MLLM for automatically discovering physical coordinates and governing equations from high-dimensional data. Specifically, we design a series of enhanced visual prompts for MLLM to enhance its spatial perception. In addition, MLLM's domain knowledge is employed to navigate the search process within the equation space. Quantitative and qualitative evaluations on two representative types of systems demonstrate that the proposed method effectively discovers the physical coordinates and equations from both simulated and real experimental data, with long-term extrapolation accuracy improved by approximately 26.96% compared to the baseline.

Introduction

Nonlinear dynamics are prevalent across numerous fields in science and engineering, such as astrophysics, fluid mechanics, and materials science (Tenachi, Ibata, and Diakogiannis 2023; Wang, Wagner, and Rondinelli 2019; Li et al. 2025c,b). Identifying the symbolic equations governing the dynamics from data is crucial for understanding and predicting such systems, a task known as symbolic regression (Langley 1981; Schmidt and Lipson 2009; Cornelio et al. 2023). Traditional symbolic regression approaches typically assume that the physical coordinates are of low dimensionality and focus on developing more efficient and accurate search algorithms (Biggio et al. 2021; Shojaee et al. 2023; La Cava et al. 2021). However, real-world scientific scenarios are often hindered by the high-dimensional nature of observational data, making it difficult to navigate the exponentially expanding symbolic space, even though a significant portion of the high-dimensional variables may be redundant (Chen et al. 2022; Pope et al. 2021). Reasoning physical

knowledge from high-dimensional observational data to facilitate predictive understanding (Liu et al. 2025; Duan et al. 2022) poses a novel and interdisciplinary challenge.

From Kepler's discovery of planetary motion laws to the most advanced symbolic regression techniques, the discovery of equations has historically relied on scientists manually processing observational data to obtain compact physical quantities in suitable coordinate systems (Chen et al. 2022; Luan, Liu, and Sun 2022). However, automatically discovering both physical coordinates and the governing equations on them from high-dimensional data is a challenging problem. With advancements in deep learning, especially visual models (Krizhevsky, Sutskever, and Hinton 2012; He et al. 2016; Dosovitskiy 2020), discovering physical laws from high-dimensional data, like videos, has become more feasible. Unsupervised motion video prediction with neural networks integrated with parameterized physical modules (e.g., neural ODE (Chen et al. 2018)) allows for implicit learning of dynamics from high-dimensional observations (Guen and Thome 2020; Wu et al. 2023; Higgins et al. 2021; Hofherr et al. 2023; Li et al. 2025a; Bounou, Ponce, and Carpentier 2021). Another approach is to embed physical engines as inductive biases into the model pipeline, compelling the neural network to infer physical quantities that satisfy the governing physical laws from video streams (Kadambi et al. 2023; Yang et al. 2022; Fotiadis et al. 2023; Kandukuri et al. 2022; Jaques, Burke, and Hospedales 2019). However, these methods separate the discovery of coordinates and equations, presuming known dynamics equations or physics engines before identifying physical quantities. Recent efforts have succeeded in jointly discovering physical coordinates and equations (Champion et al. 2019; Luan, Liu, and Sun 2022; Zhang, Liu, and Sun 2024), yet they still rely on prior knowledge of equation forms and state dimensions, limiting their generalization to unfamiliar systems.

High-dimensional data challenges traditional optimization methods like Bayesian optimization due to the lack of well-defined quantitative evaluations for intrinsic coordinates and governing equations. Large language models (LLMs) excel in problem-solving by leveraging pretrained knowledge and enhancing prompts for scientific discovery across various domains. (Boiko et al. 2023; M. Bran et al. 2024; Kang and Kim 2024). Multimodal large language models (MLLMs) with visual encoders achieve spatial un-

*Corresponding author (luyan@pjlab.org.cn).

derstanding akin to human visual intelligence. (Wu et al. 2025). Recent studies (Liu et al. 2025) show MLLMs can deduce physical properties and motion patterns from images without prior knowledge, revealing their potential in high-dimensional data. Moreover, most symbolic regression methods, based on genetic programming, search equation spaces through mutation and recombination. By leveraging the pretraining knowledge of LLM to guide this search, equation discovery can be more efficient and avoid suboptimal solutions (Shojaee et al. 2024; Ma et al. 2024). Thus, we can anticipate that a well-designed reasoning framework and visual prompts could harness MLLMs for visual perception and scientific discovery, enabling automatic identification of joint physical coordinates and governing equations.

In this work, we propose a Video Equation Reasoning framework (VER) based on multimodal large language models to automatically discover physical coordinates and their corresponding governing equations from high-dimensional data. VER first introduces a set of enhanced visual prompts designed for MLLMs to uncover the intrinsic physical coordinate space of observed data. In the equation reasoning module, we employ a hypothesis-assessment-iteration reasoning chain to refine existing symbolic regression methods for equation discovery. By integrating coordinate discovery and equation reasoning, VER is the first to explore the potential of MLLMs in equation discovery from high-dimensional data. Quantitative and qualitative evaluations on two types of representative spatiotemporal dynamical systems demonstrate that the proposed method accurately discovers the physical coordinates and governing equations from both simulated and experimental data. The extrapolation accuracy of the discovered equations improves by approximately 26.96% on average compared to the baseline.

Our contributions can be summarized as follows:

- We design a series of visual locating tools and feedback prompts for MLLMs to discover low-dimensional physical coordinates in complex spatiotemporal dynamics.
- We propose a hypothesis generation and optimization evaluation strategy that leverages MLLMs’ pretrained scientific knowledge, significantly enhancing the performance of existing methods in equation reasoning.
- Extensive experiments on representative dynamical systems demonstrates that VER surpasses existing methods by a significant margin and is capable of extracting physical insights from high-dimensional observations of real-world systems.

Problem Formulation

In the task of inferring governing equations for high-dimensional data, the goal is to find a compact and accurate symbolic expression. Here, we consider a class of video-like systems governed by low-dimensional coordinates, that is, systems whose dynamics evolve on a low-dimensional manifold (Champion et al. 2019). Given the dataset $\mathcal{D} = \{x_i\}_{i=1}^n$, where $x_i \in \mathbb{R}^D$ is the i -th observed state (i.e., a frame of video), we aim to uncover the underlying mathematical relationships such that $\frac{dx}{dt} = f(x)$. This fundamentally relies on an effective coordinate system \mathcal{Z} , in which the dynamics

have a simple low-dimensional representation $\frac{dz}{dt} = \hat{f}(z)$. Therefore, this type of problem consists of two coupled sub-problems:

- **Discovering physical coordinates** is to learning a pair of bidirectional transformations $\phi : \mathbb{R}^D \rightarrow \mathbb{R}^d$ and $\psi : \mathbb{R}^d \rightarrow \mathbb{R}^D$, which map the equation discovery in high-dimensional space $\frac{dx}{dt} = f(x)$ to the intrinsic coordinate system $\frac{dz}{dt} = g(\phi(x)) = g(z)$.
- **Reasoning governing equations** means inferring a closed-form expression for the dynamics g governing the system based on its evolution trajectory in the low-dimensional coordinate system, also known as symbolic regression.

The discovered physical coordinates directly influence the governing equation, such as the number of variables and the simplicity of the equation. A good equation should not only accurately fit the observed data points but also exhibit strong generalization capability on unseen data.

Methodology

While state-of-the-art MLLMs possess powerful visual understanding and reasoning capabilities, our approach aims to incrementally unlock their ability to infer dynamical equations from high-dimensional observational data (video modality). We propose a comprehensive reasoning framework, VER, which includes the entire Chain-of-Thought (CoT) to discover physical coordinates and reason governing equations from visual inputs, as shown in Figure 1.

Discovering physical coordinates

We consider two types of high-dimensional systems. The first type is the pixel coordinate system, where physical laws are presented in the form of Cartesian coordinates of rigidly moving objects (Luan, Liu, and Sun 2022; Zhang, Liu, and Sun 2024; Liu et al. 2025). MLLM needs to identify the intrinsic physical coordinate system by locating the trajectory of the target object’s motion through a sequence of coordinates. The second type is the more complex latent coordinate system, whose spatiotemporal evolution is governed by latent low-dimensional variables, presenting periodic or quasiperiodic oscillatory patterns (Champion et al. 2019; Rudy et al. 2017). We sample a small number of frames from the data and ask MLLM to determine their type in order to initiate different locating tools.

Detection for Pixel Coordinate Let \mathbb{L} and \mathbb{I} denote a set of language characters (prompts) and a frame of continuous video, respectively. Given a set of queries $q = \{x_l, x_i | x_l \in \mathbb{L}, x_i \in \mathbb{I}\}$ corresponding to the motion video, we aim to obtain the corresponding physical coordinate sequence $Z = \{z\}_{i=1}^n$ with the help of a frozen MLLM, working as ϕ . The coordinate sequence is retrieved through a string extractor e , which fetches substrings within specific delimiters from the historical outputs. MLLM serially traverses each query and maintains a history, including locating outputs from previous messages. Considering that visual prompting is more effective than language prompting for locating tasks, we design a locating toolkit, LocateTool, to be applied to

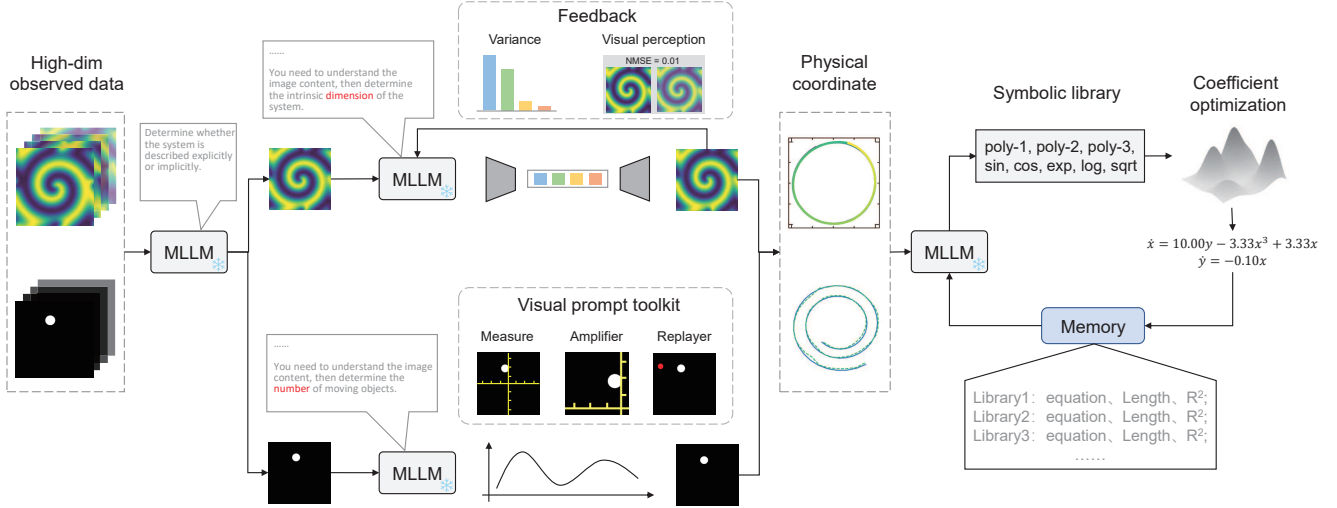


Figure 1: Overall pipeline of proposed video equation reasoning framework.

each query of MLLM, thereby enhancing MLLM’s spatial understanding through augmented visual prompts. We design three types of locating tools as enhanced visual prompts, which serve to make judgments before and after MLLM’s locating.

Spatial Measurement overlays a coordinate system with linear graduations and gridlines on the original image, providing a clearer reference for target localization. The graduations simplify the localization task, allowing MLLM to read the coordinates of the target rather than making predictions. The gridlines help MLLM further align the target with the coordinate graduations.

Regional Amplifier first calls MLLM to detect the quadrant where the target is located, then crops the area. By zooming into the local region of the target’s quadrant, MLLM observes the spatial relationship between the target and the coordinate system at close range. To avoid misidentification, MLLM is additionally called to confirm whether the cropped area contains the target object as a secondary verification.

Plot Replayer displays MLLM’s initial locating results as markers (e.g., red dots) on the original frame and calls MLLM to compare the visual discrepancy between the target object and the detection location for error correction. As a feedback iteration step in the reasoning chain, the replayer is used after the initial locating of each frame. However, for the sake of simplicity in the formula, we have incorporated it into the LocateTool functionality in Algorithm 1 in appendix.

After serially detecting the state of each frame, we introduce a filter tool to smooth the physical coordinate trajectory in order to enhance the continuity of motion between frames. Specifically, we designed a feedback correction module, Filter, based on the Savitzky-Golay filter (Savitzky and Golay 1964). We plot the recognized trajectory as a visual prompt and ask MLLM to determine the window length h and polynomial order p based on the evolution trend and periodicity of the trajectory. Each filtering re-

sult is visualized alongside the originally recognized trajectory as the visual prompt for the next iteration, until MLLM determines that the smoothing has preserved the evolution trend while maintaining inter-frame coordinate continuity. The pseudocode for serially extracting the physical coordinate sequence from the high-dimensional motion video is shown in Algorithm 1 in appendix.

Detection for Latent Coordinate The task of discovering physical coordinates in the latent coordinate system is no longer visual target localization, but rather the encoding of intrinsic variables that capture complex spatiotemporal evolution patterns (Chen et al. 2022). Here, intrinsic variables refer to the minimal set of variables that describe all the information of a dynamic system (Li, Wang, and Li 2023). Although prior work has developed manifold learning methods such as Koopman operator theory and delayed embedding (Lusch, Kutz, and Brunton 2018; Wu et al. 2024), these models heavily rely on prior assumptions about the system’s intrinsic dimensions (i.e., the number of intrinsic variables).

In this work, we use an autoencoder as an auxiliary tool to design a feedback-iteration reasoning chain for MLLM to automatically determine the intrinsic dimensions of unknown systems. Specifically, in each iteration of MLLM, we record a pair of encoder-decoder ϕ_d and ψ_d with a bottleneck dimension d and perform self-supervised reconstruction on each frame of the observed evolution trajectory $x_i \in \mathbb{R}^D$, obtaining the intrinsic variable sequence $Z = \{z\}_{i=1}^n$. We maintain an experience buffer to store the reconstruction error corresponding to the bottleneck dimension d and the reconstruction samples as the text and visual prompts for the next iteration. Furthermore, we compute the variance explained ratio $\{\frac{\lambda_i}{\sum_{j=1}^d \lambda_j}\}_{i=1}^d$ of the d -dimensional intrinsic variables, where λ_i is the eigenvalue of the i -th principal component, to enhance the prompt. The differences in the magnitude of variance contribution rates help MLLM determine whether redundant dimensions exist and decide the bottleneck dimension for the next iteration. Finally, the most

suitable bottleneck dimension d , as determined by MLLM, along with the corresponding encoder ϕ_d and decoder ψ_d , are input into the governing equation reasoning module.

Reasoning governing equations

We adopt the sparse identification method for nonlinear dynamics (SINDy) (Brunton, Proctor, and Kutz 2016) as the starting point for our approach. Inspired by the fact that latent governing equations typically contain only a finite number of terms, SINDy identifies the equations by optimizing the coefficients of predefined symbolic terms (e.g. \sin , \exp , and x^2). Specifically, SINDy defines a symbolic library $\Theta(z) = [\theta_1(z), \theta_2(z), \dots, \theta_k(z)] \in \mathbb{R}^{d \times k}$, where θ_i represents a candidate symbolic term. The symbolic library is linearly combined to form a deterministic system $\frac{dz}{dt} = \Theta(z)\Xi$, where $\Xi = [\xi_1, \xi_2, \dots, \xi_k] \in \mathbb{R}^{k \times 1}$ is the coefficient to be optimized for each symbolic term. Given the coordinate sequence $Z = \{z_i\}_{i=1}^n$ and its derivative sequence $\dot{Z} = \{\dot{z}_i\}_{i=1}^n$, SINDy minimizes the loss function

$$L_{SINDy} = \frac{1}{n} \sum_{i=1}^n \|\dot{z}_i - \Theta(z_i)\Xi\| + \eta \|\Xi\| \quad (1)$$

to ensure both fitting accuracy and sparsity.

Hypothesis generation Previous SINDy-based works have succeeded (Chen, Liu, and Sun 2021; Gao and Yan 2022), but rely on a high-quality predefined symbolic library, often needing prior system knowledge to manually filter out unnecessary terms. To address systems without prior knowledge, we design a hypothesis generation module to mine the physical knowledge pre-learned by MLLM and automatically select potential symbolic terms. The hypothesis generation step utilizes the frozen MLLM to propose diverse and promising candidate symbolic terms. At each iteration t , MLLM uses replay samples from the experience pool (Sec.) as text and visual prompts, suggesting the candidate symbolic library Θ_t .

Hypothesis Assessment After generating the candidate symbolic library hypothesis Θ_t , we utilize the detected physical coordinate data for optimization and scoring. This process involves the stochastic gradient optimization of the coefficient matrix Ξ_t and evaluating its fit. Specifically, for the pixel coordinate system, we train using the loss function from Equation 1. For the latent coordinate system, we jointly fine-tune the encoder ϕ_d , decoder ψ_d , and Ξ_t to ensure that the intrinsic physical coordinates align with the physical equation. The loss function

$$L_{AE-SINDy} = \frac{1}{n} \sum_{i=1}^n \|x_i - \psi_d(x_i)\|_2^2 + \|\nabla_{x_i}(z_i)\dot{x}_i - \Theta_t(z_i)\Xi_t\|_2^2 + \eta \|\Xi\| \quad (2)$$

coordinates the overall performance of self-supervised reconstruction and equation discovery.

We employ the R^2 metric as a quantitative measure of how well the equation fits the data. Additionally, we evaluate the number $length_t$ of symbolic terms in the equation to

quantify its simplicity. In symbolic regression tasks, the goal of maintaining equation simplicity is to avoid overfitting to the limited observational data. At this stage, the candidate symbolic library hypothesis Θ_t is assessed based on both the R^2 metric and the equation length to determine its $fitness_t$. Thus, the equation discovery process is divided into two steps: (i) constructing the symbolic library, and (ii) optimizing based on stochastic gradient using PyTorch (Kingma 2014). This process aligns with the philosophy of human scientific discovery (Ma et al. 2024; Guo et al. 2024; Huang et al. 2024), where the MLLM makes decisions on the discrete components of the SINDy symbolic library based on pretrained knowledge and prior experiences in prompts, akin to the empirical hypotheses made by human scientists during scientific discovery.

Experience management To improve the search efficiency in symbolic space and avoid local optima, we employ an experience management mechanism to enhance prompts during hypothesis generation. For each iteration, we construct a sample tuple $(\Theta_t, \Xi_t, fitness_t)$ and store it in the experience pool, thus maintaining a diverse and high-quality candidate symbolic library. In the next hypothesis generation, we collect the most recent m historical experiences as an enhanced prompt for MLLM to generate a more promising symbolic library, where m represents the receptive field. MLLM is encouraged to compare equations derived from different symbolic libraries to remove redundant symbolic terms that lead to overly complex and overfitting, while exploring other promising new symbolic terms.

We implement an early stopping mechanism to handle convergence scenarios before reaching the maximum iteration limit. Once the symbolic library suggested by MLLM reaches a threshold of repetition with samples in the experience pool, the equation inference step will be terminated. At this point, MLLM will be asked to select the best governing equation from the experience pool, using fitting accuracy and simplicity as the criteria.

Experiments

We validate VER’s advantages over baselines using two types of representative systems. For each system type, we collect simulated and real videos and use VER to extract physical insights. Additionally, we conduct robustness and ablation experiments to further discuss the benefits of each MLLM component of VER compared to existing methods.

Datasets

We evaluate the proposed method in the dynamic systems of existing studies, including the pixel coordinate system formed by the motion of interested objects according to physical laws and the latent coordinate system described by nonlinear partial differential equations.

Pixel coordinate system. We validate the effectiveness of the proposed method on the pixel coordinate system using several dynamical systems shown in Figure 2, including: *Linear*, *Cubic*, *Circular*, *Van Der Pol (VDP)*, *Glider*, and *Exp* equations. These equations include various characteristics such as linear terms, nonlinear terms, and significant

differences in time scales (Guckenheimer 1980), which together form an evaluation benchmark across different levels of difficulty. The video data is generated by simulating physical trajectories, with details provided in the Appendix .

Latent coordinate system. We select three representative reaction-diffusion equations and a real video as the latent coordinate system:

- Lambda–Omega (LO) equation (Champion et al. 2019) generates spiral wave structures featuring two oscillating spatial modes.
- Brusselator (Bruss) equation (Lopez and Atzberger 2022) models the concentration dynamics in chemical reactions, where the system’s trajectory eventually reaches a limit cycle attractor.
- Shallow-Water (Water) equation (Takamoto et al. 2022), derived from the compressible Navier-Stokes equations, describes fluid dynamics in shallow water scenarios, commonly applied in large-scale geophysical flows and tsunami simulations.
- Real video (Schmitt et al. 2024) visualizes the formation of Kármán vortex streets as water flows past a cylindrical obstacle with a Reynolds number of 171, using dye to highlight the vortex pattern.

We construct the dataset by solving the differential equations numerically. The details of the data generation are provided in Appendix .

Experimental Setup

Models. We utilize the GPT-4o (Islam and Moushi 2024) in our experiments to explore the performance of our proposed VER. We validate the improvements of VER over the basic GPT-4o in the ablation study. The penalty coefficient η in Equation 1 is set to 0.01 and we explore the performance of hyperparameter search in the appendix .

Baselines. Related works (Luan, Liu, and Sun 2022; Udrescu and Tegmark 2021) on discovering coordinates from pixel coordinate videos typically employ a combination of visual localization models and symbolic regression models. We adopt a recent work (Luan, Liu, and Sun 2022), Video-SINDy, as the baseline method for the pixel coordinate system. In addition, we also replace the coordinate encoder in Video-SINDy with SAM (Kirillov et al. 2023) as a zero-shot baseline, SAM-SINDy. For the latent coordinate system, the most relevant work (Champion et al. 2019) constructs an end-to-end model combining an autoencoder and SINDy (AE-SINDy) to interpret low-dimensional patterns in high-dimensional data. Since it requires prior knowledge of the low-dimensional space dimensions, we ensure that its dimensions are consistent with those discovered by VER.

System with Pixel Coordinate

Figure 2 shows VER’s reasoning results in the pixel coordinate system, including governing equations and inferred trajectories compared to the optimal baseline. VER uses only raw video input, without needing motion type or equation terms. VER’s trajectories closely align with ground truth over time, demonstrating MLLM’s spatial understanding

through locating prompts, as supported by (Wu et al. 2025). The inferred ODE terms perfectly match the ground truth, indicating VER’s ability to uncover intrinsic dynamics in pixel space.

We assess if VER and baseline methods’ discovered equations include all correct terms, count incorrect terms, and evaluate fitting accuracy (R^2). We numerically integrate discovered equations to predict trajectories, comparing them to real ones in Table 1. VER consistently outperforms baselines, especially in long-term predictions, where inaccuracies are magnified. This highlights VER’s superior efficiency and accuracy over traditional visual symbolic regression methods. Additionally, we collect physical motion videos from public sources to confirm VER’s reliability on real systems (Appendix).

	Method	Terms Found	Equation		Prediction	
			False Positives	R^2	$R^2@100$	$R^2@1000$
Linear	Video-SINDy	Yes	0.91 ± 0.34	0.95 ± 0.02	0.90 ± 0.03	0.87 ± 0.06
	SAM-SINDy	Yes	0.45 ± 0.13	0.90 ± 0.03	0.87 ± 0.03	0.35 ± 0.13
	VER	Yes	0.38 ± 0.22	0.96 ± 0.03	0.97 ± 0.02	0.96 ± 0.02
Cubic	Video-SINDy	No	3.52 ± 1.12	0.82 ± 0.07	0.68 ± 0.18	0.26 ± 0.19
	SAM-SINDy	No	2.17 ± 1.20	0.76 ± 0.09	0.70 ± 0.12	0.22 ± 0.18
	VER	Yes	1.41 ± 0.73	0.95 ± 0.03	0.80 ± 0.16	0.62 ± 0.28
Circular	Video-SINDy	Yes	0.31 ± 0.10	0.98 ± 0.01	0.98 ± 0.03	0.90 ± 0.10
	SAM-SINDy	Yes	0.12 ± 0.03	0.92 ± 0.01	0.99 ± 0.01	0.93 ± 0.04
	VER	Yes	0	0.99 ± 0.01	1.00 ± 0.00	0.97 ± 0.05
VDP	Video-SINDy	Yes	2.31 ± 0.65	0.89 ± 0.08	0.82 ± 0.06	0.49 ± 0.13
	SAM-SINDy	Yes	2.45 ± 0.59	0.88 ± 0.03	0.92 ± 0.04	0.67 ± 0.08
	VER	Yes	0.80 ± 0.40	0.97 ± 0.01	0.94 ± 0.02	0.73 ± 0.07
EXP	Video-SINDy	Yes	2.76 ± 0.88	0.93 ± 0.08	0.93 ± 0.02	0.90 ± 0.03
	SAM-SINDy	Yes	3.21 ± 1.17	0.95 ± 0.02	0.96 ± 0.01	0.95 ± 0.02
	VER	Yes	1.34 ± 0.29	0.99 ± 0.01	0.99 ± 0.01	0.98 ± 0.02
Glider	Video-SINDy	No	2.18 ± 0.49	0.94 ± 0.02	0.98 ± 0.01	0.91 ± 0.03
	SAM-SINDy	No	2.23 ± 0.56	0.85 ± 0.04	0.99 ± 0.04	0.32 ± 0.27
	VER	Yes	0.84 ± 0.17	0.98 ± 0.01	0.99 ± 0.01	0.92 ± 0.02

Table 1: Average performance of pixel coordinate systems over 10 runs with varying seeds. $R^2@n$ indicates R^2 for n steps. Best results are in bold.

System with Latent Coordinate

The reasoning results of VER in the latent coordinate system are presented in Figure 3, including the zero-shot inferred latent coordinate space and governing equations. VER takes observation sequences in the form of multi-channel image modalities as input and locates the intrinsic dimension of high-dimensional nonlinear partial differential equations. The results in Figure 3 show that, despite the high nonlinearity of the original equations, VER reveals the linear approximation of oscillatory patterns in the latent space spanned by the intrinsic dimensions, which is consistent with the conclusions of previous works (Champion et al. 2019). Notably, in the case of the Water system, observed sequences evolved from different initial conditions are identified as trajectories with consistent dynamics in the latent space. While VER determines that two latent coordinates are required to capture the oscillatory patterns in the observation data, the results of the equation inference module indicate that the system’s

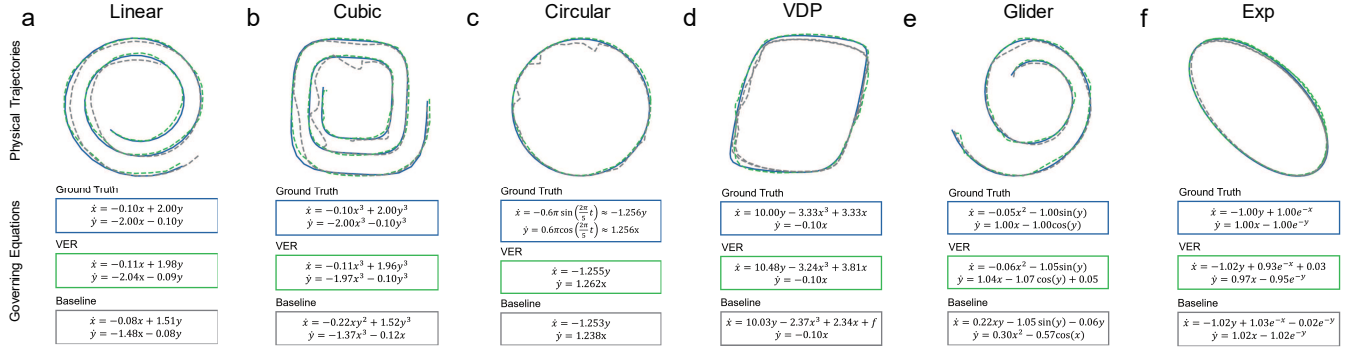


Figure 2: Reasoning results of pixel coordinate systems: blue line is ground truth; green and gray dashed lines are trajectories inferred by VER and the optimal baseline.

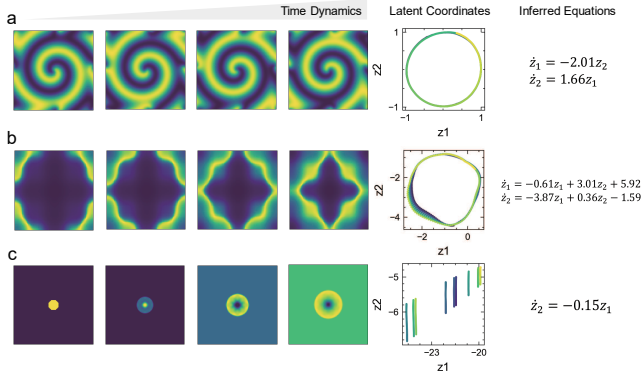


Figure 3: Reasoning results of the latent coordinate system (a) LO, (b) Bruss, and (c) Water. The trajectories show the low-dimensional oscillatory patterns found by VER.

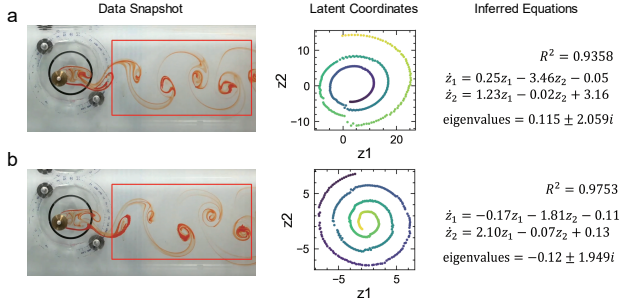


Figure 4: Kármán street video reasoning results: raw data yields vortex trajectories in (a) and (b). The red-box region's flow pattern is projected into 2D latent space.

dynamics are actually governed by a one-dimensional linear ODE. The second dimension is only used to distinguish coordinate region differences caused by varying initial conditions.

To evaluate the physical insights extracted by VER from noisy real-world systems, we extract two datasets from recorded turbulence videos, each corresponding to a fixed region over two different time intervals, as illustrated in

Figure 4. Fluctuations in incoming flow velocity or direction, as well as surface roughness of the obstacle, lead to irregular vortex shedding, resulting in the gradual breakdown of the periodic structure of the vortex street. VER successfully identifies the linear dynamics equations of oscillatory modes underlying the high-dimensional turbulent flow, which manifest as a limit cycle with a changing radius. The eigenvalues of two linear equations are $0.115 \pm 2.059i$ and $-0.120 \pm 1.949i$. The positive (negative) real parts indicate that the system state diverges from (converges to) the equilibrium over time, consistent with the spiral process shown in Figure 3. This indicates that in the first video, the vortex shedding around the cylinder exhibits an accelerating detachment trend. In the second video, the speed of vortex detachment gradually slows down. In addition, the similar imaginary parts indicate that the vortex shedding periods in two videos are close.

Robustness

We add Gaussian noise with varying strengths σ (standard deviation, mean of 0) to the observations, which biases derivative estimation and affects the accuracy and simplicity of the discovered equations. Table 6 shows the performance of all methods on the latent coordinate system. VER exhibits significantly greater robustness to noise compared to the baseline. This is because MLLM, guided by prompts, balances accuracy and equation simplicity during identification, avoiding coefficient estimation bias (overfitting) for irrelevant symbolic terms caused by noise disturbances.

Ablation Study

We conduct ablation studies to validate the contributions of VER's replaceable components to MLLM. As shown in Table 2, we evaluate several ablated versions on linear and cubic systems. Without our reasoning framework, the base MLLM (GPT-4o) fails to discover accurate equations from raw video, leading to large trajectory prediction errors. This confirms VER unlocks the MLLM's intrinsic reasoning for this task, rather than relying on potential data leakage. Ablating key components like the enhance visual prompts or the symbolic refiner (VER-SINDy) also lead to significant performance degradation or more redundant equation terms.

Thus, VER’s architecture is crucial for discovering symbolic equations from high-dimensional data. Further ablations on parameter selection (Appendix) and symbolic libraries (Fig. 5) confirm the MLLM’s superiority over traditional Bayesian methods. Finally, to test dependency on the backbone MLLM, we swap to Gemini-1.5-flash (Team et al. 2024). Although this weaker model reduces performance, it still successfully identifies the correct equation terms.

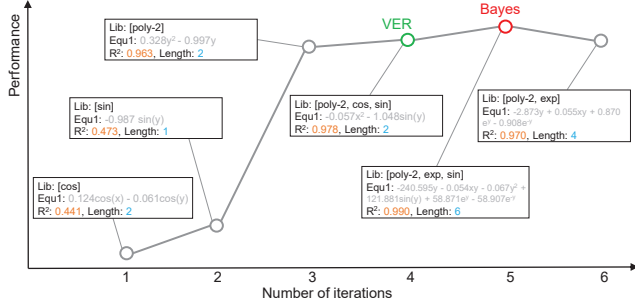


Figure 5: Comparison of VER and Bayesian optimization on *Glider* system.

	Method	Terms Found	Equation		Prediction		
			False Positives	R^2	$R^2@100$	$R^2@1000$	
Linear	GPT-4o	Yes	2.40 ± 1.36	0.25 ± 0.23	0.30 ± 0.27	0.07 ± 0.38	
	w/o measure	No	1.02 ± 0.54	0.82 ± 0.06	0.81 ± 0.05	0.70 ± 0.09	
	w/o amplifier	Yes	0.64 ± 0.31	0.91 ± 0.03	0.90 ± 0.03	0.88 ± 0.04	
	w/o replayer	Yes	0.51 ± 0.18	0.92 ± 0.01	0.93 ± 0.02	0.91 ± 0.02	
	VER-SINDy	Yes	1.25 ± 0.65	0.97 ± 0.02	0.85 ± 0.07	0.83 ± 0.07	
	VER(Gemini)	Yes	0.58 ± 0.23	0.91 ± 0.02	0.92 ± 0.03	0.89 ± 0.05	
	VER	Yes	0.38 ± 0.22	0.96 ± 0.03	0.97 ± 0.02	0.96 ± 0.02	
Cubic	GPT-4o	No	4.40 ± 1.39	0.12 ± 0.27	0.11 ± 0.25	0.06 ± 0.28	
	w/o measure	No	2.49 ± 0.82	0.87 ± 0.09	0.74 ± 0.15	0.30 ± 0.22	
	w/o amplifier	No	1.78 ± 0.62	0.91 ± 0.05	0.76 ± 0.17	0.49 ± 0.26	
	w/o replayer	Yes	1.67 ± 0.56	0.93 ± 0.04	0.75 ± 0.14	0.56 ± 0.23	
	VER-SINDy	No	2.85 ± 0.93	0.88 ± 0.07	0.71 ± 0.17	0.32 ± 0.26	
	VER(Gemini)	Yes	1.96 ± 0.74	0.90 ± 0.07	0.74 ± 0.19	0.41 ± 0.25	
	VER	Yes	1.41 ± 0.73	0.95 ± 0.03	0.80 ± 0.16	0.62 ± 0.28	

Table 2: Ablation studies on linear and cubic systems: ‘w/o’ means ‘without’. VER-SINDy uses the standard SINDy algorithm instead of VER’s inference module. VER(Gemini) uses Gemini-1.5-Flash as backbone MLLM.

Related Work

Inferring physics from video

Many studies focus on modeling video dynamics for predictive understanding, often using parameterized modules for implicit physics. Vincent et al. (Guen and Thome 2020) decoupled video content into PDE dynamics and unknowns, predicting dynamics via a parameterized PDE network. Wu et al. (Wu et al. 2023) applied stochastic PDE dynamics for real-world randomness. Hofherr et al. (Hofherr et al. 2023) and Bounou et al. (Bounou, Ponce, and Carpentier 2021) used neural ODEs and Koopman operators as dynamic predictors for interpretable parameters. These methods limit interpretability by parameterizing dynamics. With known

equations, Jaques et al. (Jaques, Burke, and Hospedales 2019) used inverse graphics to capture physical quantities, while Kandukuri et al. (Kandukuri et al. 2022) enforced rigid body mechanics via convolutional encoders to identify properties like mass and friction. Yang et al. (Yang et al. 2022) and Fotiadis et al. (Fotiadis et al. 2023) utilized encoder-decoder models for low-dimensional physical coordinates. Unlike our approach, these methods depend on prior knowledge or known equations, lacking the ability to infer physical coordinates and governing equations from unfamiliar videos.

Multimodal large language models on vision tasks

Recent research on multimodal large language models in vision tasks has demonstrated significant advancements. Wu et al. (Wu et al. 2025) meticulously designed a reasoning chain to unlock the potential of MLLMs in object detection tasks. Liu et al. (Liu et al. 2025) further combined physics engines with MLLMs, enabling MLLMs to analyze motion targets and their physical properties from images to generate physics-grounded videos. Additionally, extensive research has focused on fine-tuning or reasoning chains to enhance MLLMs’ video understanding capabilities (Zhou et al. 2024; Li et al. 2024; Zeng et al. 2024). In contrast to these efforts, we pioneer the exploration of unlocking MLLMs’ ability to discover equations from videos through carefully designed tools and reasoning chains.

Visual symbolic regression

High-dimensional symbolic regression methods for videos is a novel scientific task that typically follows two paradigms: (1) object tracking and equation discovery, where trajectories are extracted and equations identified (Luan, Liu, and Sun 2022; Zhang, Liu, and Sun 2024); (2) encoder-decoder models for latent physical coordinates, mapping data into low-dimensional spaces for equation regression (Udrescu and Tegmark 2021; Champion et al. 2019). Our approach uses MLLMs’ visual understanding and scientific knowledge for zero-shot discovery of both coordinates and equations, unifying these paradigms in one framework.

Conclusion

In this paper, we propose a video equation reasoning framework based on MLLMs to collaboratively discover physical coordinates and governing equations from high-dimensional observational data. We design an enhanced visual prompt toolkit to unify the discovery process of physical coordinates across two types of video-like systems. Extensive experiments demonstrate that the proposed method outperforms the baseline on two representative systems and provides a significant improvement to MLLMs. Additionally, the governing equations discovered by VER can quantitatively reveal the shedding period and evolving trends of vortices in real videos. In summary, this work explores the potential of MLLM in discovering scientific knowledge from multimodal data.

Limitation The performance of our framework is inherently linked to the quality of the upstream visual processing modules. Furthermore, its robustness under challenging visual conditions, such as severe occlusions or motion blur, warrants further exploration.

References

- Biggio, L.; Bendinelli, T.; Neitz, A.; Lucchi, A.; and Parascandolo, G. 2021. Neural symbolic regression that scales. In *International Conference on Machine Learning*, 936–945. Pmlr.
- Boiko, D. A.; MacKnight, R.; Kline, B.; and Gomes, G. 2023. Autonomous chemical research with large language models. *Nature*, 624(7992): 570–578.
- Bounou, O.; Ponce, J.; and Carpentier, J. 2021. Online learning and control of complex dynamical systems from sensory input. *Advances in Neural Information Processing Systems*, 34: 27852–27864.
- Brunton, S. L.; Proctor, J. L.; and Kutz, J. N. 2016. Discovering governing equations from data by sparse identification of nonlinear dynamical systems. *Proceedings of the national academy of sciences*, 113(15): 3932–3937.
- Champion, K.; Lusch, B.; Kutz, J. N.; and Brunton, S. L. 2019. Data-driven discovery of coordinates and governing equations. *Proceedings of the National Academy of Sciences*, 116(45): 22445–22451.
- Chen, B.; Huang, K.; Raghupathi, S.; Chandratreya, I.; Du, Q.; and Lipson, H. 2022. Automated discovery of fundamental variables hidden in experimental data. *Nature Computational Science*, 2(7): 433–442.
- Chen, R. T.; Rubanova, Y.; Bettencourt, J.; and Duvenaud, D. K. 2018. Neural ordinary differential equations. *Advances in neural information processing systems*, 31.
- Chen, Z.; Liu, Y.; and Sun, H. 2021. Physics-informed learning of governing equations from scarce data. *Nature communications*, 12(1): 6136.
- Cornelio, C.; Dash, S.; Austel, V.; Josephson, T. R.; Goncalves, J.; Clarkson, K. L.; Megiddo, N.; El Khadir, B.; and Horesh, L. 2023. Combining data and theory for derivable scientific discovery with AI-Descartes. *Nature Communications*, 14(1): 1777.
- Dosovitskiy, A. 2020. An image is worth 16x16 words: Transformers for image recognition at scale. *arXiv preprint arXiv:2010.11929*.
- Duan, J.; Dasgupta, A.; Fischer, J.; and Tan, C. 2022. A survey on machine learning approaches for modelling intuitive physics. *arXiv preprint arXiv:2202.06481*.
- Fotiadis, S.; Valencia, M. L.; Hu, S.; Garasto, S.; Cantwell, C. D.; and Bharath, A. A. 2023. Disentangled generative models for robust prediction of system dynamics. In *International Conference on Machine Learning*, 10222–10248. PMLR.
- Gao, T.-T.; and Yan, G. 2022. Autonomous inference of complex network dynamics from incomplete and noisy data. *Nature Computational Science*, 2(3): 160–168.
- Guckenheimer, J. 1980. Dynamics of the van der Pol equation. *IEEE Transactions on Circuits and Systems*, 27(11): 983–989.
- Guen, V. L.; and Thome, N. 2020. Disentangling physical dynamics from unknown factors for unsupervised video prediction. In *Proceedings of the IEEE/CVF conference on computer vision and pattern recognition*, 11474–11484.
- Guo, S.; Deng, C.; Wen, Y.; Chen, H.; Chang, Y.; and Wang, J. 2024. DS-Agent: Automated Data Science by Empowering Large Language Models with Case-Based Reasoning. In *Forty-first International Conference on Machine Learning*.
- He, K.; Zhang, X.; Ren, S.; and Sun, J. 2016. Deep residual learning for image recognition. In *Proceedings of the IEEE conference on computer vision and pattern recognition*, 770–778.
- Higgins, I.; Wirsberger, P.; Jaegle, A.; and Botev, A. 2021. Symetric: Measuring the quality of learnt hamiltonian dynamics inferred from vision. *Advances in Neural Information Processing Systems*, 34: 25591–25605.
- Hofherr, F.; Koestler, L.; Bernard, F.; and Cremers, D. 2023. Neural implicit representations for physical parameter inference from a single video. In *Proceedings of the IEEE/CVF Winter Conference on Applications of Computer Vision*, 2093–2103.
- Huang, Q.; Vora, J.; Liang, P.; and Leskovec, J. 2024. MLAgentBench: Evaluating Language Agents on Machine Learning Experimentation. In *Forty-first International Conference on Machine Learning*.
- Islam, R.; and Moushi, O. M. 2024. Gpt-4o: The cutting-edge advancement in multimodal llm. *Authorea Preprints*.
- Jaques, M.; Burke, M.; and Hospedales, T. 2019. Physics-as-inverse-graphics: Unsupervised physical parameter estimation from video. *arXiv preprint arXiv:1905.11169*.
- Kadambi, A.; de Melo, C.; Hsieh, C.-J.; Srivastava, M.; and Soatto, S. 2023. Incorporating physics into data-driven computer vision. *Nature Machine Intelligence*, 5(6): 572–580.
- Kandukuri, R. K.; Achterhold, J.; Moeller, M.; and Stueckler, J. 2022. Physical representation learning and parameter identification from video using differentiable physics. *International Journal of Computer Vision*, 130(1): 3–16.
- Kang, Y.; and Kim, J. 2024. ChatMOF: an artificial intelligence system for predicting and generating metal-organic frameworks using large language models. *Nature Communications*, 15(1): 4705.
- Kingma, D. P. 2014. Adam: A method for stochastic optimization. *arXiv preprint arXiv:1412.6980*.
- Kirillov, A.; Mintun, E.; Ravi, N.; Mao, H.; Rolland, C.; Gustafson, L.; Xiao, T.; Whitehead, S.; Berg, A. C.; Lo, W.-Y.; et al. 2023. Segment anything. In *Proceedings of the IEEE/CVF international conference on computer vision*, 4015–4026.
- Krizhevsky, A.; Sutskever, I.; and Hinton, G. E. 2012. Imagenet classification with deep convolutional neural networks. *Advances in neural information processing systems*, 25.
- La Cava, W.; Burlacu, B.; Virgolin, M.; Kommenda, M.; Orzechowski, P.; de Franca, F. O.; Jin, Y.; and Moore, J. H.

2021. Contemporary symbolic regression methods and their relative performance. *Advances in neural information processing systems*, 2021(DB1): 1.
- Langley, P. 1981. Data-driven discovery of physical laws. *Cognitive Science*, 5(1): 31–54.
- Li, K.; Wang, Y.; He, Y.; Li, Y.; Wang, Y.; Liu, Y.; Wang, Z.; Xu, J.; Chen, G.; Luo, P.; et al. 2024. Mvbench: A comprehensive multi-modal video understanding benchmark. In *Proceedings of the IEEE/CVF Conference on Computer Vision and Pattern Recognition*, 22195–22206.
- Li, R.; Cheng, J.; Wang, H.; Liao, Q.; and Li, Y. 2025a. Predicting the dynamics of complex system via multiscale diffusion autoencoder. *arXiv preprint arXiv:2505.02450*.
- Li, R.; Wang, H.; Ding, J.; Yuan, Y.; Liao, Q.; and Li, Y. 2025b. Predicting Dynamical Systems across Environments via Diffusive Model Weight Generation. *arXiv preprint arXiv:2505.13919*.
- Li, R.; Wang, H.; and Li, Y. 2023. Learning slow and fast system dynamics via automatic separation of time scales. In *Proceedings of the 29th ACM SIGKDD Conference on Knowledge Discovery and Data Mining*, 4380–4390.
- Li, R.; Wang, H.; Liao, Q.; and Li, Y. 2025c. Predicting the energy landscape of stochastic dynamical system via physics-informed self-supervised learning. *arXiv preprint arXiv:2502.16828*.
- Liu, S.; Ren, Z.; Gupta, S.; and Wang, S. 2025. Physgen: Rigid-body physics-grounded image-to-video generation. In *European Conference on Computer Vision*, 360–378. Springer.
- Lopez, R.; and Atzberger, P. J. 2022. GD-VAEs: Geometric dynamic variational autoencoders for learning nonlinear dynamics and dimension reductions. *arXiv preprint arXiv:2206.05183*.
- Luan, L.; Liu, Y.; and Sun, H. 2022. Distilling governing laws and source input for dynamical systems from videos. *arXiv preprint arXiv:2205.01314*.
- Lusch, B.; Kutz, J. N.; and Brunton, S. L. 2018. Deep learning for universal linear embeddings of nonlinear dynamics. *Nature communications*, 9(1): 4950.
- M. Bran, A.; Cox, S.; Schilter, O.; Baldassari, C.; White, A. D.; and Schwaller, P. 2024. Augmenting large language models with chemistry tools. *Nature Machine Intelligence*, 1–11.
- Ma, P.; Wang, T.-H.; Guo, M.; Sun, Z.; Tenenbaum, J. B.; Rus, D.; Gan, C.; and Matusik, W. 2024. Llm and simulation as bilevel optimizers: A new paradigm to advance physical scientific discovery. *arXiv preprint arXiv:2405.09783*.
- Pope, P.; Zhu, C.; Abdelkader, A.; Goldblum, M.; and Goldstein, T. 2021. The intrinsic dimension of images and its impact on learning. *arXiv preprint arXiv:2104.08894*.
- Rudy, S. H.; Brunton, S. L.; Proctor, J. L.; and Kutz, J. N. 2017. Data-driven discovery of partial differential equations. *Science advances*, 3(4): e1602614.
- Savitzky, A.; and Golay, M. J. 1964. Smoothing and differentiation of data by simplified least squares procedures. *Analytical chemistry*, 36(8): 1627–1639.
- Schmidt, M.; and Lipson, H. 2009. Distilling free-form natural laws from experimental data. *science*, 324(5923): 81–85.
- Schmitt, M. S.; Koch-Janusz, M.; Fruchart, M.; Seara, D. S.; Rust, M.; and Vitelli, V. 2024. Information theory for data-driven model reduction in physics and biology. *bioRxiv*.
- Shojaee, P.; Meidani, K.; Barati Farimani, A.; and Reddy, C. 2023. Transformer-based planning for symbolic regression. *Advances in Neural Information Processing Systems*, 36: 45907–45919.
- Shojaee, P.; Meidani, K.; Gupta, S.; Farimani, A. B.; and Reddy, C. K. 2024. Llm-sr: Scientific equation discovery via programming with large language models. *arXiv preprint arXiv:2404.18400*.
- Takamoto, M.; Praditia, T.; Leiteritz, R.; MacKinlay, D.; Alesiani, F.; Pflüger, D.; and Niepert, M. 2022. Pdebench: An extensive benchmark for scientific machine learning. *Advances in Neural Information Processing Systems*, 35: 1596–1611.
- Team, G.; Georgiev, P.; Lei, V. I.; Burnell, R.; Bai, L.; Gulati, A.; Tanzer, G.; Vincent, D.; Pan, Z.; Wang, S.; et al. 2024. Gemini 1.5: Unlocking multimodal understanding across millions of tokens of context. *arXiv preprint arXiv:2403.05530*.
- Tenachi, W.; Ibata, R.; and Diakogiannis, F. I. 2023. Deep symbolic regression for physics guided by units constraints: toward the automated discovery of physical laws. *The Astrophysical Journal*, 959(2): 99.
- Udrescu, S.-M.; and Tegmark, M. 2021. Symbolic regression: Discovering physical laws from distorted video. *Physical Review E*, 103(4): 043307.
- Wang, Y.; Wagner, N.; and Rondinelli, J. M. 2019. Symbolic regression in materials science. *MRS Communications*, 9(3): 793–805.
- Wu, T.; Gao, X.; An, F.; Sun, X.; An, H.; Su, Z.; Gupta, S.; Gao, J.; and Kurths, J. 2024. Predicting multiple observations in complex systems through low-dimensional embeddings. *Nature Communications*, 15(1): 2242.
- Wu, X.; Lu, J.; Yan, Z.; and Zhang, G. 2023. Disentangling stochastic pde dynamics for unsupervised video prediction. *IEEE Transactions on Neural Networks and Learning Systems*.
- Wu, Y.; Wang, Y.; Tang, S.; Wu, W.; He, T.; Ouyang, W.; Torr, P.; and Wu, J. 2025. Dettoolchain: A new prompting paradigm to unleash detection ability of mllm. In *European Conference on Computer Vision*, 164–182. Springer.
- Yang, T.-Y.; Rosca, J.; Narasimhan, K.; and Ramadge, P. J. 2022. Learning physics constrained dynamics using autoencoders. *Advances in Neural Information Processing Systems*, 35: 17157–17172.
- Zeng, X.; Li, K.; Wang, C.; Li, X.; Jiang, T.; Yan, Z.; Li, S.; Shi, Y.; Yue, Z.; Wang, Y.; et al. 2024. Timesuite: Improving mllms for long video understanding via grounded tuning. *arXiv preprint arXiv:2410.19702*.
- Zhang, Z.; Liu, Y.; and Sun, H. 2024. Vision-based Discovery of Nonlinear Dynamics for 3D Moving Target. *arXiv preprint arXiv:2404.17865*.

Zhou, J.; Shu, Y.; Zhao, B.; Wu, B.; Xiao, S.; Yang, X.; Xiong, Y.; Zhang, B.; Huang, T.; and Liu, Z. 2024. MLVU: A Comprehensive Benchmark for Multi-Task Long Video Understanding. *arXiv preprint arXiv:2406.04264*.

Impact Statement

This paper presents work whose goal is to advance the field of Machine Learning. There are many potential societal consequences of our work, none of which we feel must be specifically highlighted here.

Data Generation

We synthesized simulated videos of pixel coordinate systems and latent coordinate systems using Python. First, the dynamical equations for each system are predefined, consistent with those in the main text. The evolution trajectories of each pixel coordinate system are simulated using the ODE solver function provided by Scipy. The 2D variables represent the x and y coordinates of moving objects in a 2D coordinate system. For the latent coordinate system described by partial differential equations, we adopt a discretized form of ordinary differential equations to numerically solve the system on a 2D spatial grid, generating data in a video-like modality. The size of each system is described in Table 3.

For the latent coordinate systems, we utilize partial differential equations (PDEs) to model complex dynamical behaviors. The following are the specific equations and parameter settings for each system:

- Lambda–Omega (LO) equation

This system generates spiral wave structures characterized by two oscillating spatial modes. The governing equations are

$$\begin{aligned}\frac{\partial u}{\partial t} &= (1 - (u^2 + v^2))u + \beta(u^2 + v^2)v + d_1 \nabla^2 u, \\ \frac{\partial v}{\partial t} &= -\beta(u^2 + v^2)u + (1 - (u^2 + v^2))v + d_2 \nabla^2 v,\end{aligned}\quad (3)$$

where the parameters are set to $d_1 = d_2 = 0.1$ and $\beta = 1$. These equations simulate the spatial dynamics observed in wave propagation phenomena.

- Brusselator (Bruss) equation

The Brusselator models the reaction-diffusion process in chemical reactions, where the dynamic trajectory approaches a limit cycle attractor after initial transients. The equations are

$$\begin{aligned}\frac{\partial u}{\partial t} &= a - (1 + b)u + vu^2 + d_1 \nabla^2 u, \\ \frac{\partial v}{\partial t} &= bu - vu^2 + d_2 \nabla^2 v,\end{aligned}\quad (4)$$

with diffusivities set as $d_1 = 1$, $d_2 = 0.1$ and reaction rates $a = 1$, $b = 3$. This system is well-suited for studying oscillatory chemical dynamics.

- Shallow-Water (Water) equation

This system provides a framework for modeling free-surface flow problems such as tsunamis or flooding events. The equations are

$$\begin{aligned}\partial_t h + \nabla \cdot h \mathbf{u} &= 0, \\ \partial_t h \mathbf{u} + \nabla \left(\mathbf{u}^2 h + \frac{1}{2} g_r h^2 \right) &= -g_r h \nabla b.\end{aligned}\quad (5)$$

We use open-source simulation data from the related work (Schmitt et al. 2024).

Additional Results

Real-world motion video

To evaluate the physical insights obtained by VER from real-world motion, we extract a video of vertical projectile motion from a public video website¹ as additional data. Compared to synthetic videos, real data has a more complex and noisy background, which poses challenges for identifying physical coordinates. We extract a complete sequence of the projectile motion from the original video and filter out blank frames to obtain a continuous set of 27 frames. As shown in Figure 6, the experimental results demonstrate that VER accurately inferred the formula for vertical projectile motion. Notably, SAM is unable to track the motion coordinates of the moving object, and thus can not derive its motion equations.

Adaptive regularization coefficient

The regularization coefficient η in Equation 1 constrains the length of the discovered equations. Larger values enhance sparsity constraints, while smaller values explore complex equations. We add η to MLLM’s sample tuple, enabling it to select both the dictionary and based on past experience. Allowing MLLM to simultaneously adjust the dictionary and regularization coefficient is indeed a more flexible approach. Experimental results (Table 4) show that adaptive selection yields significantly better long-term predictions for systems with higher-order terms.

Bayesian hyperparameter search

In the VER framework, the Savitzky-Golay filter and the symbolic dictionary of SINDy involve parameter selection. While we design visual enhancement prompts and the empirical pool for MLLM to unlock and leverage its vast pre-trained knowledge, an alternative option is Bayesian optimization. Here, we provide a comparison with Bayesian hyperparameter search to verify the necessity of the MLLM component, including: 1) *Bayes-SINDy*: Replaces MLLM-based SINDy dictionary selection with Bayesian search (using scikit-optimize). The evaluation metric follows Equation 1; 2) *Bayes-smooth*: Uses Bayesian search to select filter parameters, evaluated by the L1 error to the original trajectory; 3) *Bayes-dim*: Replaces MLLM-based dimension selection with Bayesian search, evaluated by L2 reconstruction error on the validation set.

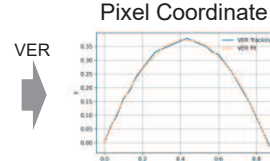
The results (Table 5) show that Bayesian search performs worse than VER. One possible explanation is that Bayesian optimization relies solely on quantitative scores, while VER also considers qualitative aspects such as equation length and visual smoothness. The lack of well-defined quantitative metrics makes this problem particularly challenging. For example, a larger symbolic dictionary may reduce fitting error but lead to overfitting. Equation complexity and fitting accuracy are often in tension, and our MLLM component is designed to balance them automatically.

¹<https://www.youtube.com/watch?v=5GiCJ5Bjupw>

	Pixel coordinate systems							Latent coordinate systems			
	Linear	Cubic	Circular	VDP	Glider	Exp	LO	Bruss	Water	Video1	Video2
Resolution	500×500	500×500	500×500	500×500	500×500	500×500	100×100	64×64	128×128	128×128	128×128
Frame	200	200	200	200	200	200	1,000	1,000	1,000	310	420

Table 3: Descriptions of dataset size.

Real Video



Ground Truth

$$\dot{y} = v_0 t - \frac{1}{2} g t^2$$

VER $R^2=0.9986$

$$\dot{y} = 1.743t - 2.031t^2$$

Figure 6: Reasoning results of the real-world motion video.

Case	Method	Terms Found	Equation False Positives	Prediction		
				R^2	$R^2@100$	$R^2@1000$
Linear	VER	Yes	0.38 ± 0.22	9.59 ± 0.25	9.68 ± 0.20	9.62 ± 0.23
	η -VER	Yes	0.35 ± 0.19	9.54 ± 0.20	9.70 ± 0.18	9.64 ± 0.22
Cubic	VER	Yes	1.41 ± 0.73	9.53 ± 0.32	7.96 ± 1.60	6.16 ± 2.78
	η -VER	Yes	1.07 ± 0.52	9.61 ± 0.26	8.45 ± 0.98	7.23 ± 2.05
Circular	VER	Yes	0	9.91 ± 0.07	9.99 ± 0.00	9.67 ± 0.45
	η -VER	Yes	0	9.92 ± 0.06	9.97 ± 0.04	9.70 ± 0.42
VDP	VER	Yes	0.80 ± 0.40	9.69 ± 0.08	9.35 ± 0.19	7.28 ± 0.72
	η -VER	Yes	0.51 ± 0.27	9.45 ± 0.05	9.52 ± 0.11	8.31 ± 0.60

Table 4: Average performance of the adaptive regularization coefficient η -VER in the pixel coordinate systems. The magnitude of R^2 is 10^{-1} .

Case	Method	Terms Found	Equation False Positives	Prediction		
				R^2	$R^2@100$	$R^2@1000$
Linear	Bayes-SINDy	Yes	0.49 ± 0.18	9.37 ± 0.41	9.42 ± 0.35	9.08 ± 0.47
	Bayes-smooth	Yes	2.51 ± 1.02	8.71 ± 0.44	8.56 ± 0.54	4.80 ± 1.22
	VER	Yes	0.38 ± 0.22	9.59 ± 0.25	9.68 ± 0.20	9.62 ± 0.23
Cubic	Bayes-SINDy	Yes	3.64 ± 1.39	9.09 ± 0.20	7.51 ± 1.48	3.63 ± 2.11
	Bayes-smooth	Yes	4.36 ± 1.96	7.72 ± 1.04	7.02 ± 1.69	2.94 ± 1.86
	VER	Yes	1.41 ± 0.73	9.53 ± 0.32	7.96 ± 1.60	6.16 ± 2.78
Glider	Bayes-SINDy	Yes	1.05 ± 0.35	9.90 ± 0.23	9.51 ± 0.14	8.33 ± 0.66
	Bayes-smooth	Yes	1.15 ± 0.30	9.15 ± 0.14	9.29 ± 0.09	7.89 ± 0.26
	VER	Yes	0.84 ± 0.17	9.78 ± 0.08	9.90 ± 0.07	9.23 ± 0.18

Table 5: Ablation studies on linear and cubic systems. Bayesian hyperparameter search replaces MLLM in selecting the SINDy dictionary (Bayes-SINDy) and smoothing parameters (Bayes-smooth). The magnitude of R^2 is 10^{-1} .

Time cost

Our approach is zero-shot, in contrast to our baseline methods that rely on case-specific tuning. Although GPT-4o introduces some network latency, which impacts our test-time comparison, our method supports parallel execution, enabling significant speed-ups through multi-process parallelism. We test time costs with varying numbers of processes P and provide a comparison with the baseline Video-SINDy, which is trained on a single RTX 4060ti GPU with Batch-size=200. The results (Figure 7) show that VER, benefiting from its parallelization advantage, is significantly faster.

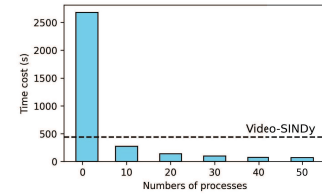


Figure 7: Time cost comparison.

Supplementary Materials

Here we provide detailed algorithms, prompts, and output examples for the methodology section.

Algorithm 1: Detection CoT for Pixel Coordinate

Input: $q = \{x_l, x_i | x_l \in \mathbb{L}, x_i \in \mathbb{I}\}$; DetTool; MLLM; Filter

Initialize an empty coordinate list and filter hyperparameters
 $Z \leftarrow \text{InitCoord}()$
 $isSmooth, h, p \leftarrow true, h_0, p_0$
 # Serially infer the physical coordinate sequence
for $i = 1$ **to** n **do**
 $q_i \leftarrow \text{DetTool}(q_i)$
 $y_i \leftarrow \text{MLLM}(q_i)$
 $Z \leftarrow Z \cup \{e(y_i)\}$
end for
 # Adaptive smoothing filter
while $isSmooth$ **do**
 # h is visual and textual prompt for smoothing results
 $Z, h \leftarrow \text{Filter}(Z, h, p)$
 $isSmooth \leftarrow \text{MLLM}(h)$
end while
Output: Z

Case	Method	Noise strength			
		$R^2@0.0$	$R^2@0.1$	$R^2@0.2$	$R^2@0.3$
LO	AE-SINDy	9.41 ± 0.04	9.06 ± 0.11	8.37 ± 0.18	7.94 ± 0.47
	VER	9.69 ± 0.06	9.57 ± 0.05	9.08 ± 0.20	8.26 ± 0.32
Bruss	AE-SINDy	8.62 ± 0.23	7.72 ± 0.44	6.91 ± 0.81	6.63 ± 0.92
	VER	8.50 ± 0.07	8.32 ± 0.18	7.68 ± 0.61	6.96 ± 0.82
Water	AE-SINDy	9.64 ± 0.08	9.00 ± 0.35	8.07 ± 0.55	7.03 ± 1.30
	VER	9.72 ± 0.10	9.66 ± 0.28	8.61 ± 0.60	7.67 ± 0.95

Table 6: The average performance of the latent coordinate system under different noise strengths, run more than 10 times with different random seeds. $R^2@σ$ is the R^2 metric, with a magnitude of 10^{-1} , of the identified equation when the noise strength is $σ$.